



Martensitic transformation of an austenitic stainless steel under non-proportional cyclic loading

Yajing Li, Dunji Yu, Bingbing Li, Xu Chen*

School of Chemical Engineering and Technology, Tianjin University, China



ARTICLE INFO

Keywords:

Martensitic transformation
Non-proportional cyclic loading
Non-proportionality of loading path
Metastable austenitic stainless steels

ABSTRACT

In this study, a series of cyclic tests on a 304L stainless steel with different loading paths were conducted. It revealed that as the non-proportionality of loading path increased, the growth rate of martensitic content became higher and its distribution among the austenitic matrix appeared more uniform. A phase transformation kinetics equation was modified to describe the effect of cumulative plastic strain, loading amplitude and loading path on martensitic transformation. A stress decomposition rule was proposed to incorporate both the non-proportional hardening and martensitic transformation hardening to describe the hardening mechanism.

1. Introduction

Several metastable austenitic stainless steels are inclined to exhibit strain-induced martensitic transformation, such as 304 stainless steels [1–11]. The transformation from face-centered cubic γ -austenite to body-centered cubic α' -martensite can occur in certain temperatures and loading conditions, leading to a significant change in mechanical properties because of the enhanced strength of α' -martensitic phase [7,8]. In recent years, martensitic transformation of stainless steel has been extensively investigated under monotonic loading (tension, compression, and torsion) [4,6,9,12–15] and uniaxial cyclic loading [1–3,7–9,16–22]. Regarding monotonic loading, the effects of chemical composition [13], plastic strain [4,6,9,12,13] etc. have been studied. For uniaxial cyclic loading martensitic transformation depends on the cyclic strain rate [7], strain amplitude [3,9,17–21] as well as cumulative plastic strain [16,17]. Also, a close relationship between cyclic deformation behavior and martensitic transformation has been demonstrated under uniaxial cyclic loading. For instance, Yu et al. [8] revealed that the remarkable secondary cyclic hardening was attributed to the increasing content of martensite, not individual phase strengthening. Similarly, Pegues et al. [7] found that the degree of total secondary hardening was correlated linearly with the content of α' -martensite.

Concerning non-proportional cyclic loading, several studies concentrated on the cyclic deformation behavior [23,24] and few on the martensitic transformation. As is known, cyclic stress response of austenitic stainless steel varies significantly under different loading paths. The smallest and largest hardening is obtained under proportional

loading path and 90° out-of-phase loading path, respectively, which is recognized as non-proportional additional hardening. Taleb and Hauet [23] explained it from the perspective of microstructural evolution. Under 90° out-of-phase loading, a series of different microstructures were compared with the proportional one, such as higher defect density, multiple slip systems, intersecting stacking faults and twins, formation of dislocation heterogeneous structure. Some researchers observed the significant difference in the cyclic deformation behavior of austenitic stainless steels under several complex loading paths [23,24]. In order to describe the effect of the loading path on the cyclic deformation behavior, a parameter called non-proportionality of the loading path was defined. The parameter can be obtained through several definitions [24–27]. Martensitic transformation was also observed during multiaxial fatigue tests. McDowell et al. [28] observed by TEM that a higher non-proportionality of the loading path could result in finer and more uniformly distributed α' -martensite for 304 stainless steel.

In summary, strain-induced martensitic transformation under monotonic and uniaxial cyclic loading has been well studied, but the research about the effect of non-proportional cyclic loading is limited yet. It is known that the loading conditions of engineering components and structures in service are complex and variable, usually resulting in multiaxial non-proportional stress state. Therefore, this study aims at investigating the martensitic transformation under non-proportional cyclic loading of 304L stainless steel.

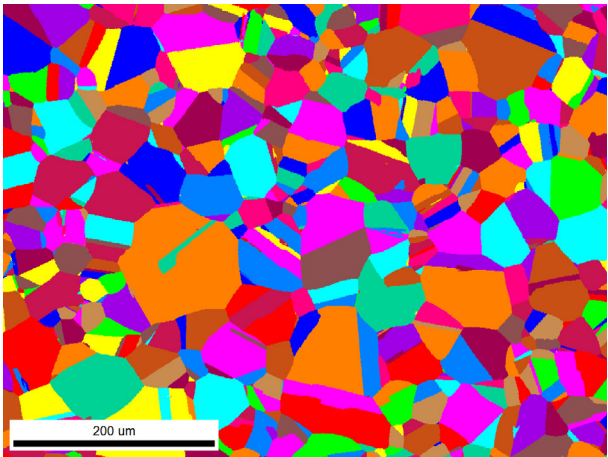
* Corresponding author.

E-mail address: xchen@tju.edu.cn (X. Chen).

Table 1

Chemical composition of the 304L stainless steel (wt %).

C	Cr	Ni	Mn	Si	P	S	Fe
0.025	18.21	8.05	1.2	0.32	0.033	0.001	Balance

**Fig. 1.** Microstructure of 304L stainless steel characterized by electron back-scatter diffraction (EBSD).

2. Experiment

The investigated material was a typical metastable austenitic stainless steel, 304L stainless steel, with its chemical composition shown in **Table 1**. The M_{d30} temperature was calculated to be 62.8 °C at which 50% of the austenite can transform into the martensite at the true strain of 30% [29]. The as-received material was provided in seamless tubes with the inner and outer diameter of 10 mm and 12.5 mm. Then solution treatment at 1050 °C for one hour followed by rapid water quench was conducted. The microstructure characterized by electron backscatter diffraction (EBSD) shows nearly equiaxed austenitic grains with a small quantity of annealing twins, as presented in **Fig. 1**. The average grain size was about $50 \pm 10 \mu\text{m}$. The mechanical properties under monotonic tensile loading were listed in **Table 2**.

The thin-walled tubular specimens (see **Fig. 2**) were designed for all cyclic tests. To remove the detrimental effects on martensitic transformation induced by machining, prior to experiments the surface of each specimen was polished to a final roughness of $\sim 0.5 \mu\text{m}$. All the tests were conducted on an MTS axial-torsional testing system at room temperature with a tension-torsional extensometer of gauge length 25 mm to measure and control the strain. Owing to the fact that martensitic transformation can be inhibited when the temperature increases [10,30], the low frequency of 0.25 Hz was employed during the cyclic tests according to Ref. [11].

Symmetrical strain-controlled cyclic experiments with various loading amplitudes and loading paths were carried out to investigate cyclic deformation behavior and martensitic transformation. Five loading amplitudes ranging from 0.4% to 1.0% were conducted in uniaxial cyclic tests, and eight loading paths were employed with a constant equivalent strain amplitude of 0.5%, as shown in detail in

Table 2

Mechanical properties under monotonic tensile loading of the 304L stainless steel.

Young's modulus, E (GPa)	Yield strength, R _{p0.2} (MPa)	Tensile strength, R _m (MPa)	Elongation, δ (%)	Reduction in area, RA (%)
193	259	642	78	56

Table 3. The loading paths were categorized as two groups, proportional loading path and non-proportional loading path. The proportional loading path included Uniaxial, Torsional and Proportional loading path, with unchanged maximum principal strain plane during cyclic loading. On the contrary for the other five non-proportional loading paths, the maximum principal strain planes changed with time continuously. To describe the effect of the loading path on the cyclic behavior, the definition and calculation methods of non-proportionality of loading path were proposed by some researchers, such as Kanazawa et al. [24], Itoh et al. [25], Chen et al. [26] and Borodii et al. [27]. According to the references, the non-proportionality values of the eight loading paths were obtained, as shown in **Table 4**. One can discover that the non-proportionality values for the three proportional loading paths are 0 no matter which definition was employed. Whereas different non-proportionality values can be obtained for any non-proportional loading path through diverse definitions. When Kanazawa model was used, it's found that the non-proportionality value for Square loading path is larger than that of Circular loading path. It is conflicted with the experimental results that the largest non-proportional additional hardening was observed under Circular loading path. In terms of Chen model, it can't distinguish Cross loading path and Rhombus loading path, which had different degrees of non-proportional additional hardening for 304L stainless steel. While both of Itoh model and Borodii model can distinguish various loading paths properly. Furthermore, Itoh model is more popular owing to its concise form and clear physical meaning as well as its superior performance in distinguishing various loading paths. Consequently, the definition put forward by Itoh et al. [25] was adopted hereinafter.

The amount of martensitic transformation was determined by a magnetic induction measuring method through a Ferritescope FMP30. The instrument can capture all ferromagnetic components and then output the result in ferrite number (FN-%). The undeformed 304L stainless steel had a single austenitic structure with almost no ferrite structure. When subjected to plastic deformation, part of the austenite in the sample may transform into martensitic structure, resulting in an increase in FN. During all the cyclic tests, three FN were randomly obtained in one cycle during the loading process. The average value of the three data, FN_{stress}, was taken as FN of the sample with stress. However, due to the negative magnetostriction, or the Villari effect, the magnetic permeability of ferromagnetic components is reduced when subjected to tension due to the rotation and reorientation of magnetic domains with applied force [13]. In order to reduce the effect of the Villari effect on magnetic permeability measurement, the sample must be macroscopically stress-free during the measurement [13]. For the Uniaxial, Torsional, and Proportional cyclic tests, the sample can be unloaded at certain number of cycles to measure FN under stress-free state, but it can't be achieved for non-proportional cyclic tests because of the non-synchronously varying axial stress and shear stress. Therefore, a uniaxial cyclic test with the strain amplitude of 0.5% was carried out to solve the problem. During the selected cycles (600, 1200, 1800, 2400, 3000, 3600, and 4200) of the test, the FN of the sample were acquired under three different stress states, including the maximum tensile stress state, the maximum compressive stress state, and stress-free state, denoted by FN_{max_ten_stress}, FN_{max_com_stress}, and FN_{stress-free}, respectively. Then the relation between FN with and without macroscopic stress was obtained. Based on the relation, FN with macroscopic stress, FN_{stress}, was corrected to that without macroscopic stress, FN_{stress-free}. Then the volume fraction of α'-martensite, ξ, was estimated from FN_{stress-free}, using the following equation:

$$\xi = k \cdot FN_{stress-free} \quad (1)$$

where k is the conversion factor from vol.% ferrite to vol.% α'-martensite. It was determined to be 1.7 according to the Ref. [31].

The microstructure investigations were carried out using electron backscatter diffraction (EBSD) (Edax) equipped on a field-emission

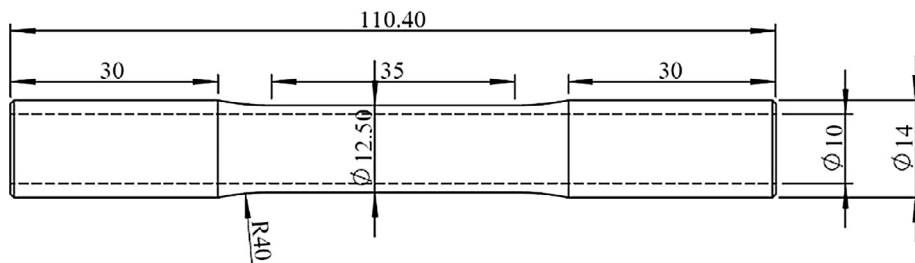


Fig. 2. Tubular specimen geometry of 304L stainless steel.

scanning electron microscopy (FE-SEM, Hitachi SU5000) at 30 kV. Specimens were loaded to a certain number of cycles in order to ensure the same cumulative plastic strain of 2 mm/mm. Afterwards, small longitudinal sections were cut from the gauge section of the deformed specimens and then mechanically ground and finally polished with a colloidal silica suspension (OP-S, Struers). In order to eliminate the effect of potential martensitic transformation of the surface materials during mechanical polishing, electrochemical polishing was carried out before EBSD observation to obtain the intrinsic surface of the sample. The as-received specimen (denoted by AR) was also characterized as a reference. The analyzed area was $600 \mu\text{m} \times 450 \mu\text{m}$ containing more than 200 grains in order to be statistically representative. The scanning step was as small as $0.8 \mu\text{m}$ to acquire high-quality microstructural morphology.

3. Results and discussion

3.1. Cyclic deformation behavior

Fig. 3 illustrates cyclic deformation behavior under various loading paths. It is characterized by peak equivalent stress versus the number of

Table 3

Detailed description of the loading paths carried out in present study with a constant equivalent strain amplitude of 0.5%.

Loading Path Name	Loading Path Sketch	Waveform	Loading Path Name	Loading Path Sketch	Waveform
Uniaxial			Torsional		
Proportional			Ladder		
Cross			Rhombus		
Square			Circular		

Table 4

The value of non-proportionality of loading paths according to different definitions.

	Kanazawa [25]	Itoh [24]	Chen [26]	Borodii [27]
Uniaxial	0	0	0	0
Torsional	0	0	0	0
Proportional	0	0	0	0
Ladder	0.25	0.1	0.06	0.24
Cross	0.87	0.34	0.44	0.64
Rhombus	0.87	0.77	0.44	0.89
Square	0.99	0.77	0.63	0.85
Circular	0.87	1	0.75	1

Note: Poisson ratio was 0.5 during the calculation.

cycles on a semi-logarithmic coordinate system. The equivalent stress σ_{eq} is defined according to von-Mises criterion:

$$\sigma_{\text{eq}} = \sqrt{\sigma^2 + 3\tau^2} \quad (2)$$

where σ and τ represent axial stress and shear stress in the mid-section of the specimen gage section, respectively. One can remark that the

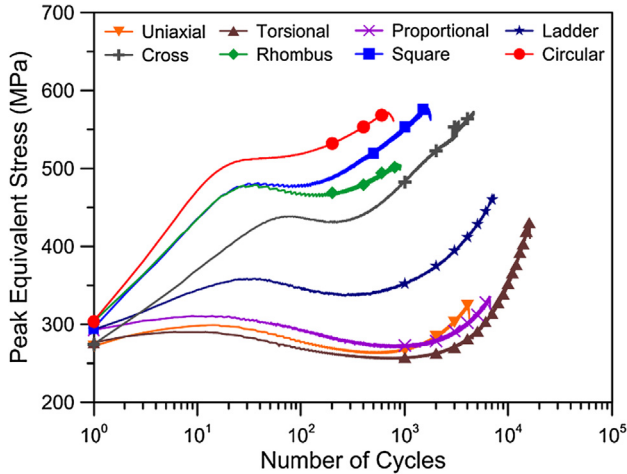


Fig. 3. Cyclic stress response of the cyclic tests subjected to various loading paths.

material exhibited three-staged cyclic stress response regardless of the loading path, initial hardening for the first few cycles, then cyclic saturation (only for Circular loading path specimen) or softening for a period of time, finally followed by a distinct secondary hardening until final failure. The initial hardening has been reported to relate to an increase of the total dislocation density, whereas cyclic saturation or softening is attributed to the movement and re-arrangement of dislocations [32]. Then, the explanation for secondary hardening mainly focuses on the martensitic transformation by some researchers [7,8], which will be discussed subsequently.

In order to compare the relative magnitude of initial hardening, cyclic softening and secondary hardening subjected to various loading paths, three expressions are given as follows:

$$R_{IH} = (\sigma_{IH} - \sigma_0)/\sigma_0 \quad (3)$$

$$R_{SO} = (\sigma_{SO} - \sigma_0)/\sigma_0 \quad (4)$$

$$R_{SH} = (\sigma_{SH} - \sigma_0)/\sigma_0 \quad (5)$$

where R_{IH} , R_{SO} and R_{SH} are defined as initial hardening ratio, cyclic softening ratio and secondary hardening ratio, respectively. σ_0 , σ_{IH} , σ_{SO} and σ_{SH} are the stress value at the first cycle, maximum stress value reached during initial hardening stage, minimum stress value achieved during the cyclic softening stage, maximum stress value attained during secondary hardening stage, respectively, which are illustrated schematically in Fig. 4(a).

The relationship between the degree of initial hardening, cyclic softening, secondary hardening and the non-proportionality of the loading path are represented in Fig. 4(b)–(d). The initial hardening ratio, cyclic softening ratio and secondary hardening ratio were all positively related to the non-proportionality of loading path, indicating the close relationship between cyclic stress responses and the loading path. The phenomenon is known as non-proportional additional hardening and has been reported in other austenitic stainless steels [23,25]. The non-proportional loading path results in the rotation of maximum shear strain plane, causing more grains to undergo their most favorable orientation for slip. Then, more dislocation interactions and entanglements develop, and additional hardening is found [26]. Higher defect density is also responsible for the non-proportional additional hardening of the material, including multiple slip systems, shear bands, interacting stacking faults and twins [24,28].

3.2. Microstructure by EBSD characterization

To characterize the crystallographic features of microstructures under various cyclic loadings, EBSD observations were performed on six

specimens, including one with the as-received condition and five deformed specimens subjected to Uniaxial, Ladder, Cross, Square and Circular loading path. The grain boundary distribution maps (Fig. 5) and phase maps (Fig. 6) were obtained to analyze the discrepancies among the specimens.

Fig. 5 illustrates grain boundary distribution maps, with low angle grain boundaries (LAGBs) in red and high angle grain boundaries (HAGBs) in black. A clear difference of LAGBs can be observed among the six specimens. For the as-received specimen, there was little amount of LAGBs. For the specimens of Proportional and Ladder loading path with non-proportionality of 0 and 0.1, the amount of LAGBs was still very small, indicating low dislocation density. A small amount of LAGBs occurred in Cross loading path with non-proportionality of 0.34. For Square loading path with non-proportionality of 0.77, more amount of LAGBs was observed. A large number of LAGBs were generated in Circular loading path with non-proportionality of 1.

Fig. 6 shows phase maps with γ -austenite in green, α' -martensite in red and ϵ -martensite in yellow. It is clear that hardly any ϵ -martensite was observed for each specimen. It's reported that the ϵ -martensite appeared as an intermediate phase during $\gamma \rightarrow \epsilon \rightarrow \alpha'$ transformation, and its amount initially increased and then decreased during tensile deformation process of 304 stainless steel [33,34]. However, such $\gamma \rightarrow \epsilon \rightarrow \alpha'$ transformation was not captured by in situ neutron diffraction during uniaxial cyclic loading of a 304 stainless steel [8], which was consistent with the EBSD observations in this study. Therefore, it is reasonable to deduce that α' -martensite is the main product of martensitic phase transformation under cyclic loading. Its amount and the distribution in the austenitic matrix are further examined as below. For the as-received specimen, only a single austenitic structure was observed and no martensitic phase was found. In addition, there was little amount of α' -martensite in Proportional and Ladder specimens. However, for the three other specimens, the amount of blocky-shaped α' -martensite was increasing successively along with the non-proportionality of loading path. Meanwhile, significant differences of α' -martensitic distribution can also be observed. Specifically, for Cross specimen, almost all the α' -martensite was distributed along the austenitic grain boundaries. While for Square one, α' -martensite was distributed mainly along the grain boundaries but some at the interior of the grains. Yet, it was distributed uniformly along the grain boundaries as well as the interior of the grains for Circular loading path.

The amount of LAGBs and α' -martensite of specimens subjected to various loading paths is quantitatively assessed in Fig. 7. From this figure, a positive correlation was demonstrated between the fraction of LAGBs as well as α' -martensite and the non-proportionality of loading path. Sakane et al. [35] reported that under the same principal strain range, the greater the non-proportionality, the more complex the dislocation structures and the greater number of dislocation cells. Thus, one can deduce that for the loading path with larger non-proportionality, more dislocation interactions and dislocation tangles can be generated. Then the regions with high concentrations of LAGBs are enlarged, accompanied with higher fault density, thus promoting the nucleation and development of α' -martensite. Hecker et al. [36] observed a similar phenomenon in monotonic experiments in which the balanced biaxial tension can form more amount of martensite than uniaxial tension in the same von-Mises equivalent strain.

The distribution of α' -martensite in the austenite matrix tended to be more uniform with the increase of the non-proportionality of loading path under the same cumulative plastic strain. A reasonable explanation is that when the non-proportionality of loading path is relatively small, the dislocation density near the grain boundaries is much larger than in the interior of grains. As the non-proportionality increases, a large number of dislocations can be observed both along the grain boundaries and in the interior of grains, leading to more uniformly distributed α' -martensite nucleation sites. As a result, the α' -martensite is uniformly distributed in the austenitic grain boundaries and the interior of grains. The similar phenomenon was reported in [28] that the

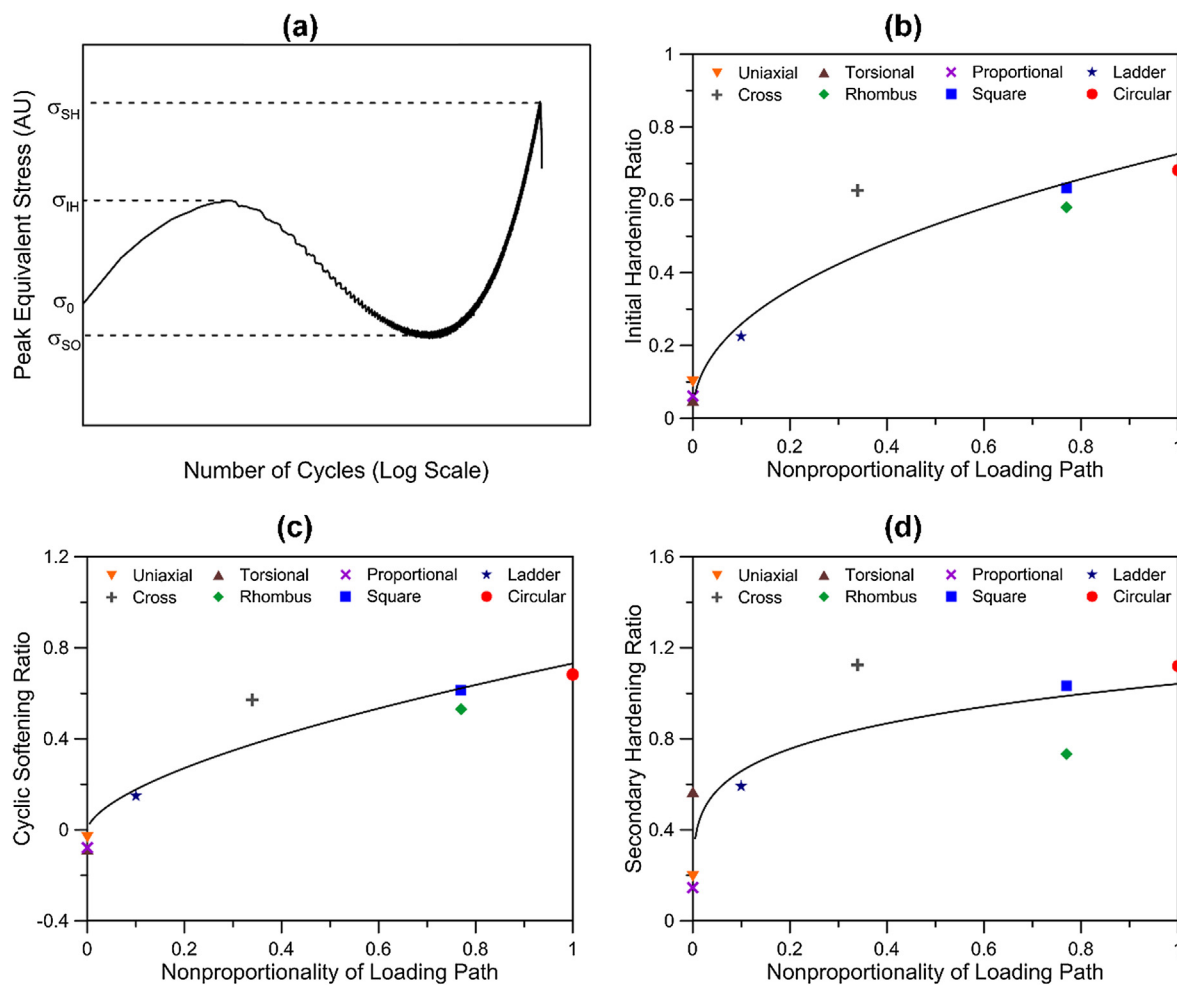


Fig. 4. (a) Schematic diagram of the four stresses involved in Eqs. (3)–(5). Relationship between the degree of (b) initial cyclic hardening (c) cyclic softening (d) secondary cyclic hardening and the non-proportionality of loading path.

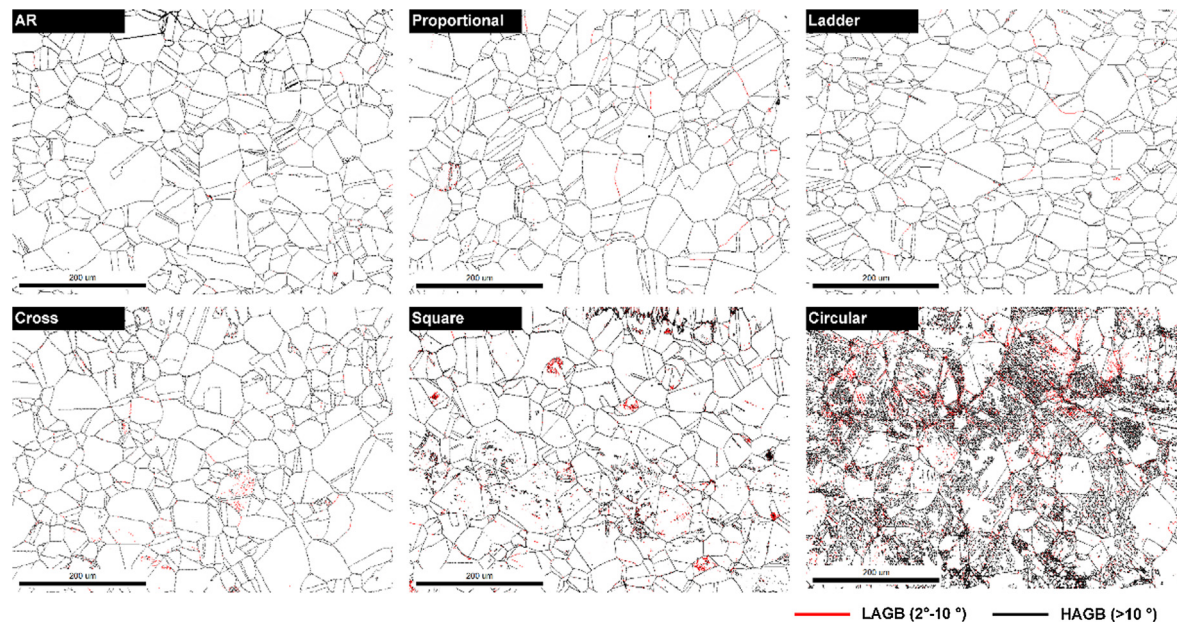


Fig. 5. Grain boundary distribution maps of specimens using EBSD subjected to different loading paths with cumulative plastic strain 2 mm/mm. (Note: the specimen axis is horizontal.)

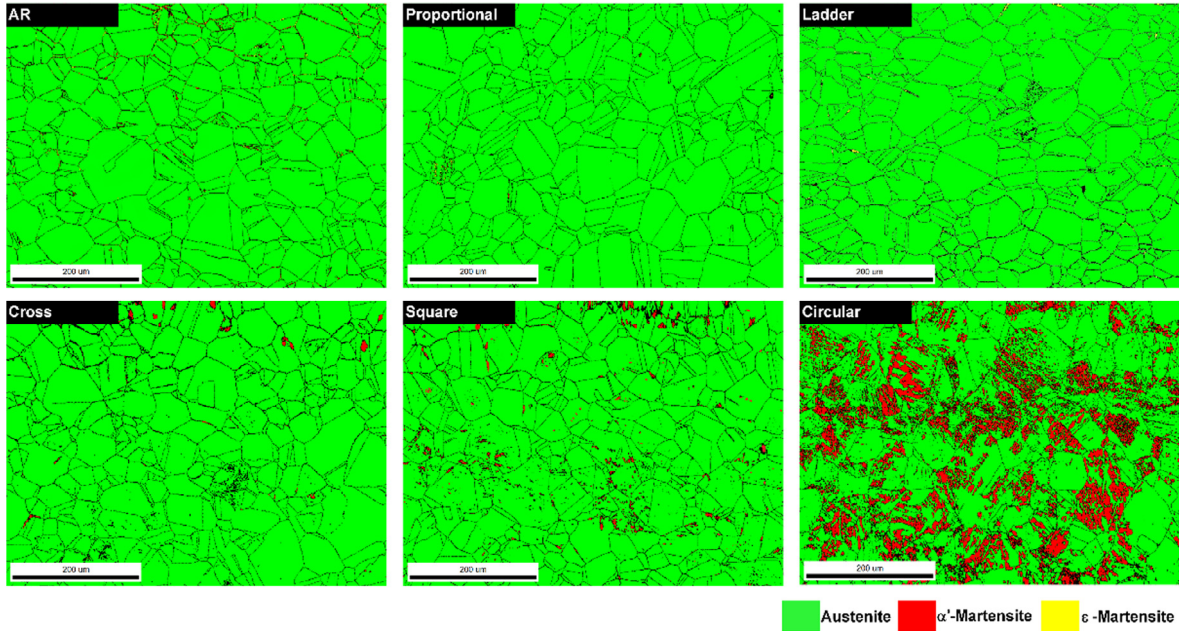


Fig. 6. Phase maps of specimens using EBSD subjected to different loading paths with cumulative plastic strain 2 mm/mm. (Note: the specimen axis is horizontal.)

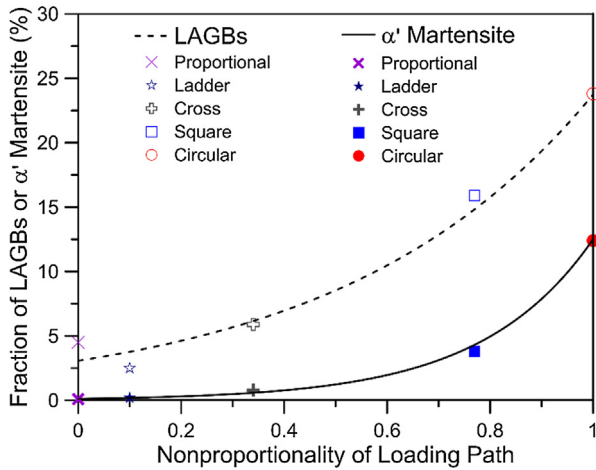


Fig. 7. Fraction of low angle grain boundaries (LAGBs) and α' -martensite of different specimens obtained by EBSD at the same cumulative plastic strain.

α' -martensite was more uniformly distributed among austenitic matrix for complex cyclic loading path compared with uniaxial loading.

3.3. Modified phase transformation kinetics equation

Fig. 8 shows the result of FN of uniaxial cyclic test with strain amplitude of 0.5%. FN under the maximum tensile stress state, the maximum compressive stress state, and stress-free state in selected cycles of the sample is displayed in Fig. 8(a). Among the three data of each selected cycle, $FN_{\text{stress-free}}$ were the largest, followed by $FN_{\text{max_ten_stress}}$, and finally $FN_{\text{max_com_stress}}$. It can be explained by the Villari effect. Fig. 8(b) displayed the relation between $FN_{\text{stress-free}}$ and $FN_{\text{max_ten_stress}}$ as well as $FN_{\text{max_com_stress}}$. Two linear relations can be fitted as following:

$$FN_{\text{stress-free}} = 1.12FN_{\text{max_ten_stress}} \quad (6)$$

$$FN_{\text{stress-free}} = 1.24FN_{\text{max_com_stress}} \quad (7)$$

It can be reasonably inferred that the FN under stress-free state is 1.12 to 1.24 times the FN randomly measured in one cycle during

loading. On average, the following relation can be calculated:

$$FN_{\text{stress-free}} = 1.18FN_{\text{stress}} \quad (8)$$

where FN_{stress} is the FN with stress. By using the relation, the FN under stress state can be corrected to that under stress-free state with maximum error deviation under 5%. Thereafter, the volume fraction of α' -martensite can be calculated from $FN_{\text{stress-free}}$ employing Equation (1).

To describe the martensitic transformation evolution during cyclic process, the volume fraction of α' -martensite versus cumulative plastic strain is given in Fig. 9. The cumulative plastic strain was calculated as:

$$\lambda = \int_0^t \left(\frac{2}{3} \dot{\varepsilon}_{ij}^P \dot{\varepsilon}_{ij}^P \right)^{1/2} dt \quad (9)$$

where $\dot{\varepsilon}_{ij}^P$ is plastic strain rate.

The cumulative plastic strain can directly affect the martensitic transformation of 304L. It's indicated from Fig. 9(a) and (b) that for each cyclic test, almost no α' -martensite (less than 1% defined here) was generated before the cumulative plastic strain reaching a critical value. After that, the volume fraction of α' -martensite increased with the cumulative plastic strain obviously. The tendency is consistent with the results of uniaxial cyclic tests reported before [9,18,37]. As reported in Refs. [5,10,14], during the initial stage of plastic deformation, dislocation structures such as shear bands, stacking faults, ϵ -martensite and twins appear. Later, these dislocation structures gradually develop, and when the micro-shear band thickness reach a critical size of 5–7 nm, stable α' -martensitic embryos begin to form [30,38]. Subsequently, the α' -martensitic embryos begin to entangle with each other, thus forming stable α' -martensitic structures. With the cumulative plastic strain increasing progressively, an increasing quantity of α' -martensitic nucleation sites form, leading to a rapid increase of martensitic α' -content.

The martensitic transformation is not only dependent on the cumulative plastic strain, but also the strain amplitude and the loading path significantly, as shown in Fig. 9(a) and (b). With the increase of the strain amplitude and the non-proportionality of loading path, a higher growth rate of martensitic volume fraction as a function of cumulative plastic strain was observed. Moreover, the critical value of cumulative plastic strain initiating martensitic transformation decreased with increasing strain amplitude and the non-proportionality of loading path, just as illustrated in Fig. 9(c) and (d). A similar

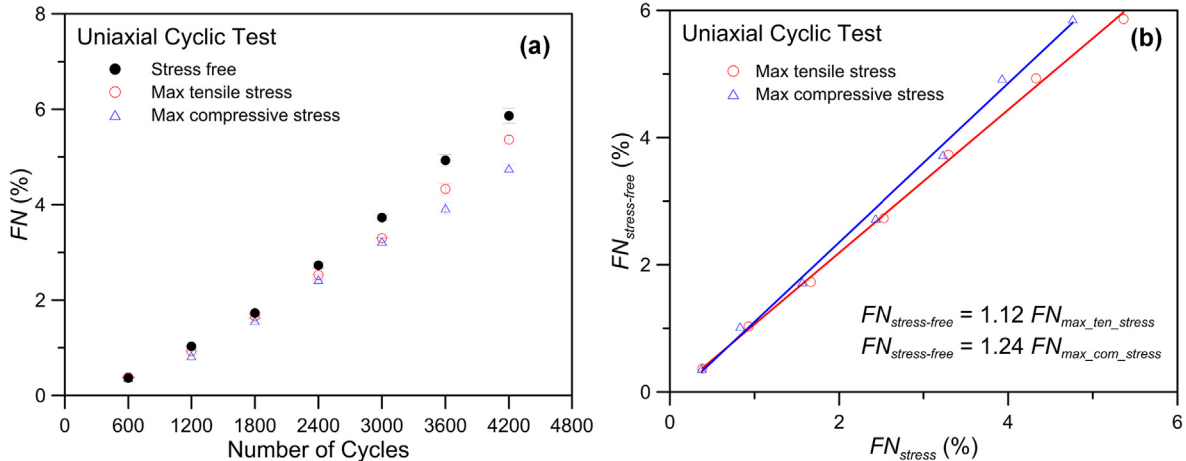


Fig. 8. The result of ferrite number (FN) of uniaxial cyclic test with strain amplitude of 0.5%. (a) FN under three different stress states in selected cycles. (b) Relation between the FN under stress-free state, $FN_{\text{stress-free}}$, and that under the maximum tensile stress state, $FN_{\text{max_ten_stress}}$, as well as the maximum compressive stress state, $FN_{\text{max_com_stress}}$.

phenomenon has been discovered in uniaxial cyclic tests by some researchers [9,18].

A phase transformation kinetics equation was proposed by Smaga et al. [18] to describe the α' -martensitic content evolution as a function of cumulative plastic strain under uniaxial cyclic loading in metastable

austenite stainless steel:

$$\xi = \xi_{\text{max}} (1 - e^{-\alpha \lambda^n}) \quad (10)$$

where ξ is the volume fraction of α' -martensitic, λ is the cumulative plastic strain, ξ_{max} is the saturation value of the volume fraction of α' -

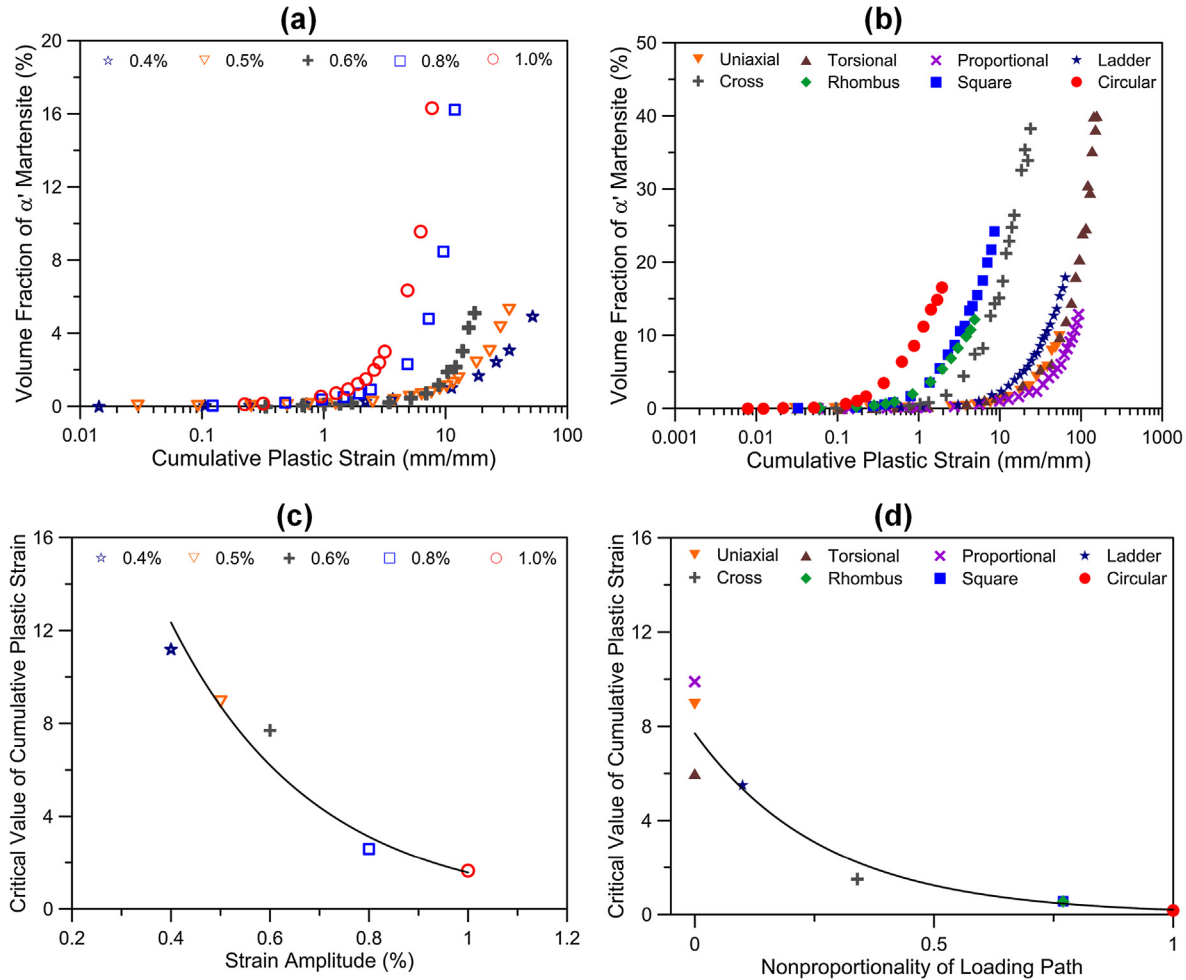


Fig. 9. Evolution of volume fraction of α' -martensite with cumulative plastic strain (a) under uniaxial cyclic loading with different strain amplitudes (b) under various loading paths with equivalent strain amplitude of 0.5%. Correlation between the critical value of cumulative plastic strain initiating martensitic transformation and the (c) strain amplitude (d) non-proportionality of loading path.

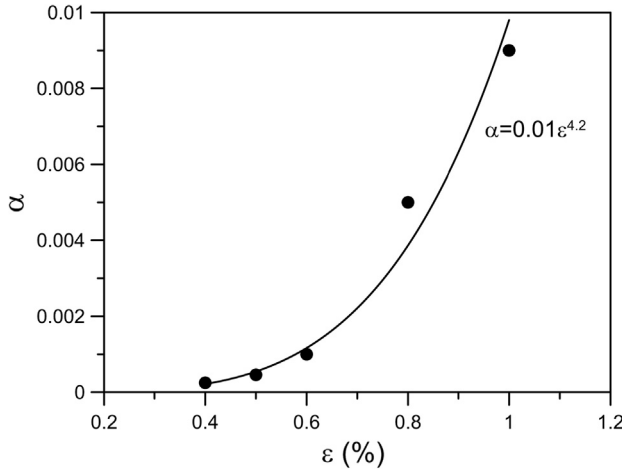


Fig. 10. The relationship between the parameter α and the strain amplitude ε (%) fitted by a power equation.

martensitic, n is a material constant for each stainless steel related to the austenitic stability, and α is used to describe the effect of strain amplitude on martensitic transformation. When α is given a very tiny value, the martensitic content will increase at a rate close to zero, thus leading to nearly no martensitic transformation. The equation has been employed successfully in Ref. [18] to describe the martensitic transformation under uniaxial cyclic loading with various strain amplitudes.

In current study, it is found that the martensitic transformation is related to the loading path in addition to the cumulative plastic strain and strain amplitude. Therefore, it's necessary to improve the Smaga's equation to describe the three effects on the martensitic transformation simultaneously. The new equation is presented as follows:

$$\xi = \xi_{\max} \left(1 - e^{-\alpha e^{D\phi} \lambda^n} \right) \quad (11)$$

where the term $e^{D\phi}$ is coupled into Smaga's equation to consider the effect of loading path on the martensitic transformation, D is a fitting parameter, ϕ is the non-proportionality of loading path calculated by Itoh's definition given in Table 4. Fig. 10 gives the relationship between the calibrated parameter α and the strain amplitude ε (%) which was fitted by a power equation well. The equation can be expressed as follows:

$$\alpha = 0.01\varepsilon^{4.2} \quad (12)$$

For every strain amplitude, ξ_{\max} is 100% and n is 1.35. The resulting transformation kinetics plot are shown in Fig. 11(a). For the cyclic tests

subjected to different loading paths with the equivalent strain amplitude of 0.5%, the values of parameter ξ_{\max} , α and n used the same data as the uniaxial cyclic test with strain amplitude of 0.5%. The parameter D can be obtained by Circular experimental data with a value of 5.16. The resulting transformation kinetics plot subjected to different loading paths are displayed in Fig. 11(b).

For the uniaxial cyclic tests in Fig. 11(a), the difference in parameter α lead to the difference in the curves with different strain amplitudes. While for Fig. 11(b), the difference in the curves with different loading paths is due to parameter ϕ . The maximum martensitic value ξ_{\max} can't be reached owing to the fatigue failure of the specimens. The calculation results by the equation for Uniaxial, Torsional, and Proportional loading path cyclic tests are identical owing to their same non-proportionality value. It is really same for true for Rhombus and Square loading path as non-proportionality definition. For the cyclic test with a larger strain amplitude or non-proportionality of loading path, the curve obtained by the equation is steeper, corresponding to a larger martensitic transformation rate. In summary, the modified phase transformation kinetics equation can reflect the effect of the cumulative plastic strain, strain amplitude and loading path on the martensitic transformation.

3.4. Hardening mechanism under non-proportional loading path

To explore the hardening mechanism under non-proportional loading path, the correlation between peak equivalent stress and volume fraction of α' -martensite is displayed during the initial stage and the secondary hardening stage in Fig. 12. Here, the initial stage refers to the combination of initial hardening and cyclic softening or saturation stages. It is obviously noticed that during the initial stage there is less than 1% α' -martensite and no explicit relation existed between peak equivalent stress and the volume fraction of α' -martensite. Different peak equivalent stress is observed under various loading paths, which can be attributed to non-proportional additional hardening. In contrast, during the secondary hardening stage, an interesting phenomenon is observed that for all loading paths, peak equivalent stress increases linearly with the volume fraction of α' -martensite. This is because the strength of α' -martensite is greater than that of austenite. No matter which loading path, the increase in α' -martensite content leads to the same degree of hardening of the material. It is indicated that martensitic transformation rather than non-proportionality of the loading makes a significant effect on the secondary hardening. In brief, the hardening mechanism under two stages is different: the non-proportional additional hardening accounted for the initial stage whereas the martensitic transformation hardening dominated during the secondary

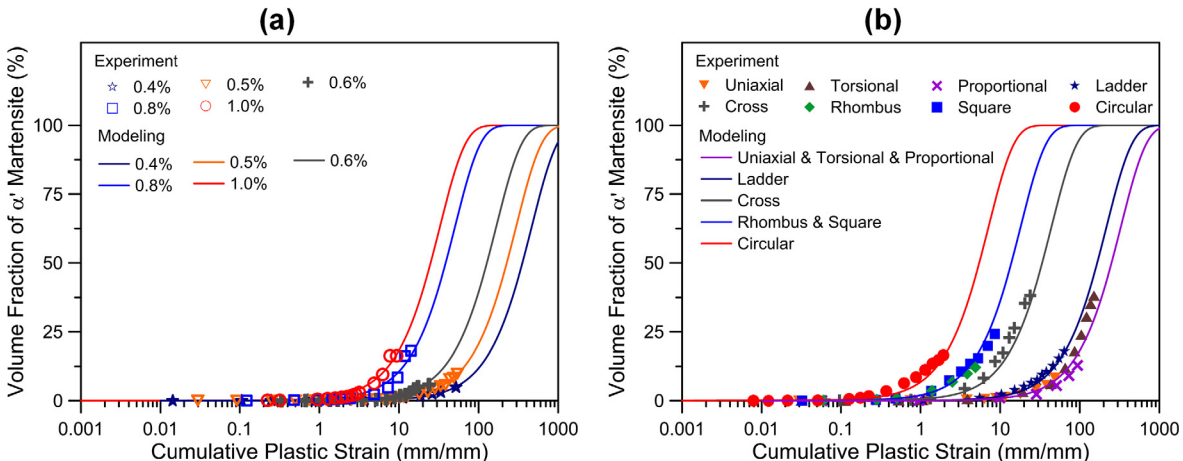


Fig. 11. Comparison of martensitic transformation evolution between the results by the modified equation (solid lines) and the experimental data (symbols) of (a) uniaxial cyclic tests with various strain amplitudes (b) cyclic tests subjected to different loading paths with a constant equivalent strain amplitude.

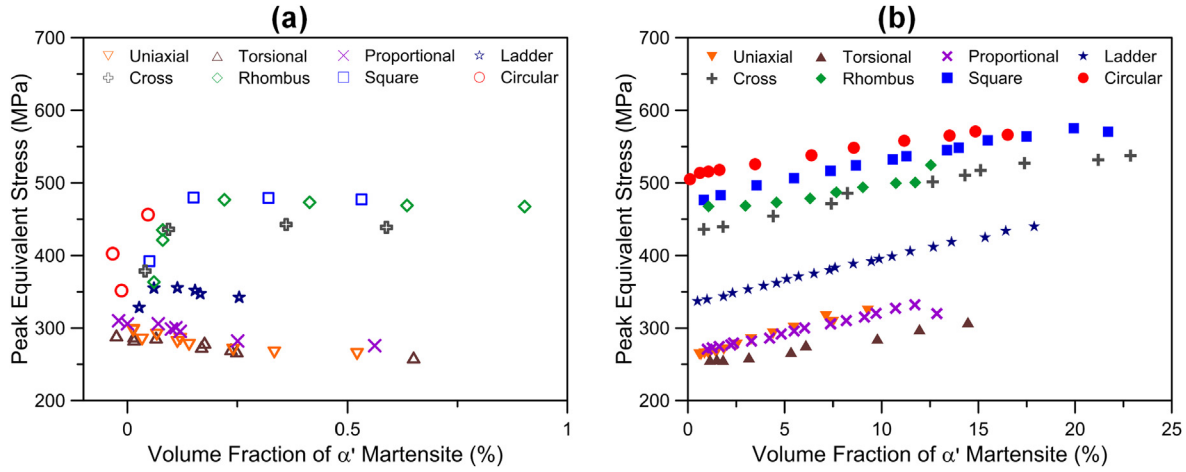


Fig. 12. Correlation between cyclic stress response and martensitic transformation during (a) initial stage and (b) secondary hardening stage.

hardening stage.

Taking these results into consideration, a stress decomposition rule is proposed for the secondary stage. The stress can be decomposed into two parts associated with non-proportional hardening and martensitic transformation hardening, respectively, as follows:

$$\sigma = \sigma_{\text{non}} + \sigma_{\text{mar}} \quad (13)$$

$$\sigma_{\text{non}} = \sigma(\phi) = A\phi^B + \sigma_{\text{uni}} \quad (14)$$

$$\sigma_{\text{mar}} = \sigma(V_{\alpha}) = KV_{\alpha} \quad (15)$$

where the first part σ_{non} is the peak equivalent stress at the beginning of the secondary hardening, representing the non-proportional additional hardening due to the difference of the non-proportionality of loading path. The relationship between σ_{non} and non-proportionality of loading path ϕ can be expressed by Eq. (14) and fitted by a power law relationship. σ_{uni} is the peak equivalent stress at the beginning of the secondary hardening of Uniaxial loading path cyclic test. A and B are both materials constants. Four sets of experimental data ϕ - σ_{non} , including Uniaxial, Ladder, Square and Circular results, are used to determine the parameter A and B, as shown in Fig. 13(a). The second part σ_{mar} is the peak equivalent stress owing to the increase of α' -martensite content which is only related to the volume fraction of α' -martensite V_{α} . The parameter K is a constant and it is obtained by averaging the slope values of experimental results from the eight cyclic tests. The values of all the parameters involved in Eq. (14) and (15) are listed in Table 5. Fig. 13(b) shows that the proposed stress decomposition rule

Table 5
Parameters of the equivalent stress model in Eqs. (14) and (15).

A (MPa)	B	σ_{uni} (MPa)	K (MPa/%)
242.5	0.5	263.41	4.869

can describe the cyclic stress response subjected to different loading paths well.

4. Conclusions

A series of uniaxial and multiaxial cyclic tests on a 304L stainless steel were carried out to investigate the effect of the loading amplitude and loading path on the martensitic transformation. The following conclusions can be drawn.

- (1) The 304L stainless steel exhibited initial cyclic hardening, cyclic softening or saturation and significant secondary cyclic hardening subjected to each loading path. The non-proportional additional hardening was observed, and its magnitude increased with the non-proportionality of loading path.
- (2) The significant difference of the content and distribution of α' -martensite was observed among the specimens with the same cumulative plastic strain but subjected to different cyclic loading paths. The content of α' -martensite increased with the increase of

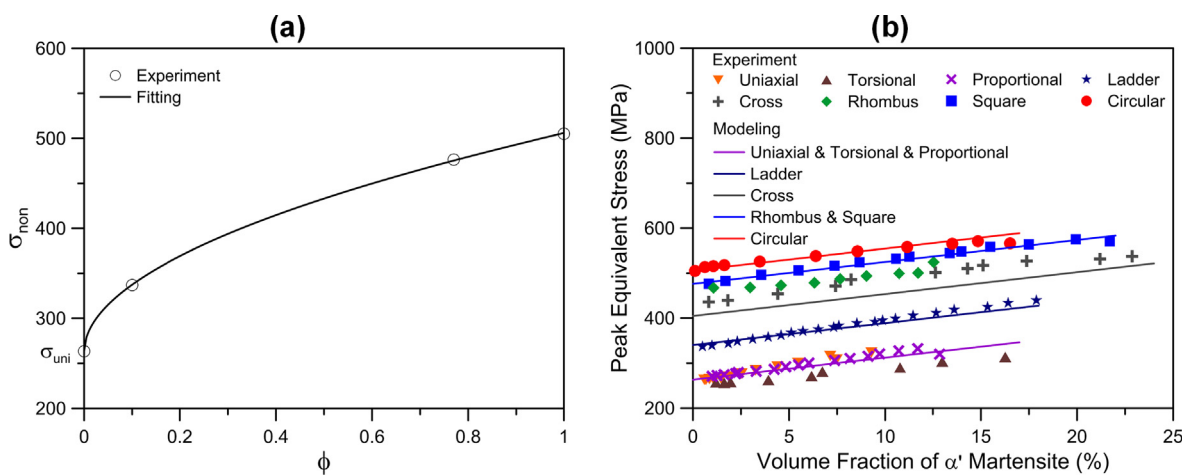


Fig. 13. (a) Fitting the relation of σ_{non} and ϕ in Eq. (14). (b) Comparison of the results calculated by the proposed model (solid lines) and the experimentally determined martensitic contents (data points) of the correlation between cyclic stress response and martensitic transformation.

- non-proportionality of loading path. For the specimen subjected to small non-proportionality of loading path, α' -martensite mainly developed along the grain boundaries and twin boundaries. While for the Circular loading path, it preferably formed uniformly at the interior of the austenitic grains and along the austenitic grain boundaries.
- (3) The martensitic transformation under cyclic loading can be generated only when the cumulative plastic strain exceeded a critical value. The magnitude of the critical value was inversely related to the loading amplitude and the non-proportionality of loading path. As the loading amplitude and the non-proportionality increased, the growth rate of α' -martensitic volume fraction became higher. A phase transformation kinetics equation was improved to take into account the effects of cumulative plastic strain, loading amplitude and loading path simultaneously. The results calculated by the equation were in excellently consistent with the experimental results.
- (4) The hardening mechanism of 304L stainless steel under non-proportional cyclic loading is different during initial and secondary hardening stages. The non-proportional hardening contributed to the additional hardening during the initial stage, while the martensitic transformation mainly accounted for the secondary hardening stage. Based on these observations, a stress decomposition rule to incorporate non-proportional hardening and martensitic transformation hardening was proposed which described the hardening mechanism of 304L stainless steel under non-proportional cyclic loading well.

Acknowledgements

The authors gratefully acknowledge financial support for this work from the National Key Research and Development Program of China (No. 2017YFC0805600) and the National Natural Science Foundation of China (No. 51435012).

Appendix A. Supplementary material

Supplementary data to this article can be found online at <https://doi.org/10.1016/j.ijfatigue.2019.03.020>.

References

- [1] Paul SK, Stanford N, Hilditch T. Austenite plasticity mechanisms and their behavior during cyclic loading. *Int J Fatigue* 2018;106:185–95. <https://doi.org/10.1016/j.ijfatigue.2017.10.005>.
- [2] Gonchar AV, Mishakin VV, Klyushnikov VA. The effect of phase transformations induced by cyclic loading on the elastic properties and plastic hysteresis of austenitic stainless steel. *Int J Fatigue* 2018;106:153–8. <https://doi.org/10.1016/j.ijfatigue.2017.10.003>.
- [3] Dey R, Tarafder S, Sivaprasad S. Influence of phase transformation due to temperature on cyclic plastic deformation in 304LN stainless steel. *Int J Fatigue* 2016;90:148–57. <https://doi.org/10.1016/j.ijfatigue.2016.04.030>.
- [4] Ahmedabadi PM, Kain V, Agrawal A. Modelling kinetics of strain-induced martensite transformation during plastic deformation of austenitic stainless steel. *Mater Design* 2016;109:466–75. <https://doi.org/10.1016/j.matdes.2016.07.106>.
- [5] Liu J, Chen C, Feng Q, Fang X, Wang H, Liu F, et al. Dislocation activities at the martensite phase transformation interface in metastable austenitic stainless steel: an in-situ TEM study. *Mater Sci Engng A* 2017;703:236–43. <https://doi.org/10.1016/j.msea.2017.06.107>.
- [6] Das YB, Forsey AN, Simm TH, Perkins KM, Fitzpatrick ME, Gungor S, et al. In situ observation of strain and phase transformation in plastically deformed 301 austenitic stainless steel. *Mater Design* 2016;112:107–16. <https://doi.org/10.1016/j.matdes.2016.09.057>.
- [7] Pegues JW, Shao S, Shamsaei N, Schneider JA, Moser RD. Cyclic strain rate effect on martensitic transformation and fatigue behaviour of an austenitic stainless steel. *Fatigue Fract Eng M* 2017;40:2080–91. <https://doi.org/10.1111/ffe.12627>.
- [8] Yu D, An K, Chen Y, Chen X. Revealing the cyclic hardening mechanism of an austenitic stainless steel by real-time in situ neutron diffraction. *Scr Mater* 2014;89:45–8. <https://doi.org/10.1016/j.scriptamat.2014.06.021>.
- [9] Zeng W, Yuan H. Mechanical behavior and fatigue performance of austenitic stainless steel under consideration of martensitic phase transformation. *Mater Sci Eng A* 2017;679:249–57. <https://doi.org/10.1016/j.msea.2016.10.005>.
- [10] Hahnberger F, Smaga M, Eifler D. Microstructural investigation of the fatigue behavior and phase transformation in metastable austenitic steels at ambient and lower temperatures. *Int J Fatigue* 2014;69:36–48. <https://doi.org/10.1016/j.ijfatigue.2012.07.004>.
- [11] Pessoa DF, Kirchhoff G, Zimmermann M. Influence of loading frequency and role of surface micro-defects on fatigue behavior of metastable austenitic stainless steel AISI 304. *Int J Fatigue* 2017;103:48–59. <https://doi.org/10.1016/j.ijfatigue.2017.05.018>.
- [12] Souza Filho IR, Zilnyk KD, Sandim MJR, Bolmaro RE, Sandim HRZ. Strain partitioning and texture evolution during cold rolling of AISI 201 austenitic stainless steel. *Mater Sci Eng A* 2017;702:161–72. <https://doi.org/10.1016/j.msea.2017.07.010>.
- [13] Wang Z, Beese AM. Effect of chemistry on martensitic phase transformation kinetics and resulting properties of additively manufactured stainless steel. *Acta Mater* 2017;131:410–22. <https://doi.org/10.1016/j.actamat.2017.04.022>.
- [14] Shen YF, Li XX, Sun X, Wang YD, Zuo L. Twinning and martensite in a 304 austenitic stainless steel. *Mater Sci Eng A* 2012;552:514–22. <https://doi.org/10.1016/j.msea.2012.05.080>.
- [15] Schloth P, Weisser MA, Van Swygenhoven H, Van Petegem S, Susila P, Subramanya Sarma V, et al. Two strain-hardening mechanisms in nanocrystalline austenitic steel: an *in situ* synchrotron X-ray diffraction study. *Scr Mater* 2012;66:690–3. <https://doi.org/10.1016/j.scriptamat.2012.01.021>.
- [16] Bayerlein M, Christ HJ, Mughrabi H. Plasticity-induced martensitic transformation during cyclic deformation of AISI 304L stainless steel. *Mater Sci Eng A* 1989;114:111–6. [https://doi.org/10.1016/0921-5093\(89\)90871-X](https://doi.org/10.1016/0921-5093(89)90871-X).
- [17] Ye D, Xu Y, Xiao L, Cha H. Effects of low-cycle fatigue on static mechanical properties, microstructures and fracture behavior of 304 stainless steel. *Mater Sci Eng A* 2010;527:4092–102. <https://doi.org/10.1016/j.msea.2010.03.027>.
- [18] Smaga M, Walther F, Eifler D. Deformation-induced martensitic transformation in metastable austenitic steels. *Mater Sci Eng A* 2008;483–484:394–7. <https://doi.org/10.1016/j.msea.2006.09.140>.
- [19] Das A. Dislocation configurations through austenite grain misorientations. *Int J Fatigue* 2015;70:473–9. <https://doi.org/10.1016/j.ijfatigue.2014.06.012>.
- [20] Das A. Magnetic properties of cyclically deformed austenite. *J Magn Magn Mater* 2014;361:232–42. <https://doi.org/10.1016/j.jmmm.2014.02.006>.
- [21] Das A, Sivaprasad S, Chakraborti PC, Tarafder S. Morphologies and characteristics of deformation induced martensite during low cycle fatigue behaviour of austenitic stainless steel. *Mater Sci Eng A* 2011;528:7909–14. <https://doi.org/10.1016/j.msea.2011.07.011>.
- [22] Dutta K, Sivaprasad S, Tarafder S, Ray KK. Influence of asymmetric cyclic loading on substructure formation and ratcheting fatigue behaviour of aisi 304LN stainless steel. *Mater Sci Eng A* 2010;527:7571–9. <https://doi.org/10.1016/j.msea.2010.07.107>.
- [23] Taleb L, Hauet A. Multiscale experimental investigations about the cyclic behavior of the 304L SS. *Int J Plast* 2009;25:1359–85. <https://doi.org/10.1016/j.ijplas.2008.09.004>.
- [24] Kanazawa K, Miller KJ, Brown MW. Cyclic deformation of 1% Cr-Mo-V steel under out-of-phase loads. *Fatigue Fract Mater Struct* 1979;2:217–28. <https://doi.org/10.1111/j.1460-2695.1979.tb01357.x>.
- [25] Itoh T, Sakane M, Ohnami M, Socie DF. Nonproportional low cycle fatigue criterion for type 304 stainless steel. *Int J Fatigue* 1995;19:438. [https://doi.org/10.1016/S0142-1123\(97\)90066-9](https://doi.org/10.1016/S0142-1123(97)90066-9).
- [26] Chen X, Gao Q, Sun XF. Low-cycle fatigue under non-proportional loading. *Int J Fatigue* 1996;16:221–5. [https://doi.org/10.1016/0142-1123\(94\)90007-8](https://doi.org/10.1016/0142-1123(94)90007-8).
- [27] Borodii MV, Strizhalo VA. Analysis of the experimental data on a low cycle fatigue under nonproportional straining. *Int J Fatigue* 2000;22:275–82. [https://doi.org/10.1016/S0142-1123\(00\)00005-0](https://doi.org/10.1016/S0142-1123(00)00005-0).
- [28] McDowell DL, Stahl DR, Stock SR, Antolovich SD. Biaxial path dependence of deformation substructure of type 304 stainless steel. *Metall Trans A* 1988;19:1277–93. <https://doi.org/10.1007/BF02662589>.
- [29] Angel T. Formation of martensite in austenitic stainless steels, effect of deformation, temperature and composition. *J Iron Steel Inst* 1954:165–74.
- [30] Staudhammer KP, Murr LE, Hecker SS. Nucleation and evolution of strain-induced martensitic (b.c.c.) embryos and substructure in stainless steel: a transmission electron microscope study. *Acta Metall* 1983;31:267–74. [https://doi.org/10.1016/0001-6160\(83\)90103-7](https://doi.org/10.1016/0001-6160(83)90103-7).
- [31] Talonen J, Asporen P, Hänninen H. Comparison of different methods for measuring strain induced α' -martensite content in austenitic steels. *Mater Sci Technol* 2004;20:1506–12. <https://doi.org/10.1179/026708304X4367>.
- [32] Pham MS, Solenthaler C, Janssen KGF, Holdsworth SR. Dislocation structure evolution and its effects on cyclic deformation response of AISI 316L stainless steel. *Mater Sci Eng A* 2011;528:3261–9. <https://doi.org/10.1016/j.msea.2011.01.015>.
- [33] Cakmak E, Choo H, An K, Ren Y. A synchrotron X-ray diffraction study on the phase transformation kinetics and texture evolution of a TRIP steel subjected to torsional loading. *Acta Mater* 2012;60:6703–13. <https://doi.org/10.1016/j.actamat.2012.08.040>.
- [34] De AK, Murdock DC, Mataya MC, Speer JG, Matlock DK. Quantitative measurement of deformation-induced martensite in 304 stainless steel by X-ray diffraction. *Scr Mater* 2004;50:1445–9. <https://doi.org/10.1016/j.scriptamat.2004.03.011>.
- [35] Sakane M, Itoh T, Kida S, Ohnami M, Socie D. Dislocation structure and non-proportional hardening of type 304 stainless steel. *Eur Struct Integrity Soc* 1999;25:130–44. [https://doi.org/10.1016/S1566-1369\(99\)80012-0](https://doi.org/10.1016/S1566-1369(99)80012-0).
- [36] Hecker SS, Stout MG, Staudhammer KP, Smith JL. Effects of strain state and strain rate on deformation-induced transformation in 304 stainless steel: Part I. Magnetic measurements and mechanical behavior. *Metall Trans A* 1982;13:619–26. <https://doi.org/10.1007/BF02644427>.
- [37] Baudry G, Pineau A. Influence of strain-induced martensitic transformation on the low-cycle fatigue behavior of a stainless steel. *Mater Sci Eng* 1977;28:229–42. [https://doi.org/10.1016/0025-5416\(77\)90176-8](https://doi.org/10.1016/0025-5416(77)90176-8).
- [38] Olson GB, Cohen M. A mechanism for the strain-induced nucleation of martensitic transformations. *J Less Common Metals* 1972;28:107–18. [https://doi.org/10.1016/0022-5088\(72\)90173-7](https://doi.org/10.1016/0022-5088(72)90173-7).